

Stimulated Brillouin Scattering in layered media: nanoscale enhancement of silicon

M. J. A. Smith,^{1,2,*} C. Wolff,³ C. G. Poulton,² and C. M. de Sterke¹

¹*Institute of Photonics and Optical Science (IPOS),*

School of Physics, The University of Sydney, NSW 2006, Australia

²*School of Mathematical and Physical Sciences, University of Technology Sydney, NSW 2007, Australia*

³*Center for Nano Optics, University of Southern Denmark, Campusvej 55, DK-5230 Odense M, Denmark*

(Dated: November 28, 2018)

We report a theoretical study of Stimulated Brillouin Scattering (SBS) in general anisotropic media, incorporating the effects of both acoustic strain and local rotation in all calculations. We apply our general theoretical framework to compute the SBS gain for layered media with periodic length scales smaller than all optical and acoustic wavelengths, where such composites behave like homogeneous anisotropic media. We theoretically predict that a layered medium comprising nanometre-thin layers of silicon and As_2S_3 glass possesses a bulk SBS gain of $1.28 \times 10^{-9} \text{ W}^{-1} \text{ m}$. This is more than 500 times larger than the gain coefficient of silicon, and substantially larger than the gain of As_2S_3 . The enhancement is due to a combination of roto-optic, photoelastic, and artificial photoelastic contributions in the composite structure.

Interactions between photons and phonons represent an important avenue of research in contemporary photonics and optomechanics [1–3], not only for the transmission of light in optical fibres [4, 5], but also for the design of efficient, small-scale optical devices [6]. One of the most important effects for driving these interactions is Stimulated Brillouin Scattering (SBS) [5]. In bulk materials, SBS is frequently described as the resonant excitation of the first acoustic pressure mode of the medium by the optical pump field; the pressure wave acts as a travelling diffraction grating which scatters the pump and induces a Doppler-shifted returning (Stokes) wave. A significant issue with this description is that it only holds in optically isotropic media where bulk SBS interactions are only possible with longitudinal acoustic waves and not with shear acoustic waves. In materials possessing optical anisotropy, shear acoustic waves and mixed-polarised acoustic waves are also SBS-active [7–9], due to reduced symmetry constraints [10]. Here we consider SBS more generally than is frequently described, defining the process as the inelastic resonant excitation of a bulk acoustic mode by the pump wave, leading to the formation of a backwards-propagating optical Stokes wave. A key issue with SBS in technologically relevant materials platforms, such as silicon, is intrinsically low SBS gain, which motivates considerable interest in novel designs for its enhancement (i.e., [1]). In recent years, composite materials have been explored theoretically as a means of controlling SBS [11–15].

In this work, we present results for SBS in a layered medium, as shown in Fig. 1, where in addition to photoelastic processes (including artificial photoelasticity [16], see below), we also have contributions to the SBS gain from induced optical anisotropy. By incorporating all relevant optoacoustic processes, we show that the gain coefficient of layered media takes values

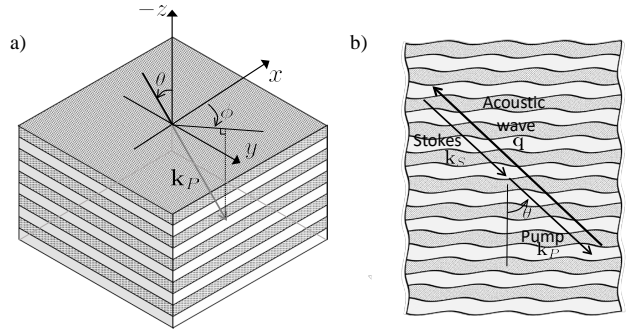


FIG. 1. (a) Illustration of composite bulk medium comprising As_2S_3 glass (white) and silicon (grey) layers with (b) cross-section view showing pump \mathbf{k}_P , Stokes \mathbf{k}_S , and acoustic \mathbf{q} wave vectors involved in bulk backwards SBS interaction.

well above the SBS gain of the constituents in bulk. To demonstrate this point, we present results for a Si- As_2S_3 layered medium, where we find a gain coefficient of $g_P = 1.28 \times 10^{-9} \text{ W}^{-1} \text{ m}$. Our gain value is two orders of magnitude larger than that of pure Si_{100}Ge ($g_P = 2.4 \times 10^{-12} \text{ W}^{-1} \text{ m}$ [13]), 75% larger than that of pure As_2S_3 ($g_P = 7.4 \times 10^{-10} \text{ W}^{-1} \text{ m}$ [17]), and an order of magnitude larger than results for a suspension of As_2S_3 spheres in Si ($g_P = 1.06 \times 10^{-10} \text{ W}^{-1} \text{ m}$ [14]). To the authors' knowledge this is the first study of SBS in layered media.

Such enhancements are achieved due to changes in the permittivity under changes in filling fraction (*artificial photoelastic* contributions), as well as changes to the permittivity under infinitesimal rotation (*roto-optic* contributions [7, 18–21]), in addition to *intrinsic* photoelastic contributions from the layers [16].

As an optoacoustic process, roto-opticity is not new [18], but is much less well-known than conventional photoelasticity, as rotationally induced birefringence is not observed in materials of high symmetry. Artificial photoelastic effects are much more recent and were discovered by the authors in 2015 [11]. All microscopic-

* michael.j.smith@sydney.edu.au

scale interactions are implicitly captured in the effective medium treatment, and are contained within the artificial electrostriction contributions (see discussion in Smith *et al.* [16]). The nontrivial relationship between radiation pressure and artificial electrostriction is demonstrated by the fact that artificial contributions vanish in the absence of either a permittivity or stiffness contrast [16], whereas radiation pressure effects vanish in the absence of only a permittivity contrast [22]. In materials possessing optical isotropy and acoustic anisotropy, such as Germanium, a material frame rotation has been shown to improve the confinement of longitudinal acoustic modes for SBS [23].

We begin by presenting a generalisation of the coupled-mode approach in Wolff *et al.* [22] for evaluating the SBS gain of uniform anisotropic media. Assuming linear constitutive behaviour in both the optical and acoustic properties, the SBS gain coefficient (in the absence of irreversible forces) is defined as [22]

$$g_P = \frac{2\omega\Omega\gamma^2}{\mathcal{I}_P\mathcal{I}_S\mathcal{I}_A\alpha}, \quad (1)$$

where γ (units [Pa]) denotes the total electrostrictive coefficient, \mathcal{I}_P is the pump intensity (units [W/m²]), \mathcal{I}_S is the Stokes intensity (units [W/m²]), and \mathcal{I}_A is the acoustic intensity (units [W/m²]), where all intensities are associated with the modes of the optical and acoustic waves in the material. Here, α is the acoustic attenuation constant (units [1/m]). These are given by

$$\gamma = -\varepsilon_0 \varepsilon_{im} \varepsilon_{jn} P_{mnlk} (\partial_l u_k)^* E_i^P (E_j^S)^*, \quad (2a)$$

$$\mathcal{I}_P = 2 (\hat{v}_g^P)_i \varepsilon_{ijk} (E_j^P)^* H_k^P, \quad (2b)$$

$$\mathcal{I}_S = 2 (\hat{v}_g^S)_i \varepsilon_{ijk} (E_j^S)^* H_k^S, \quad (2c)$$

$$\mathcal{I}_A = -2i\Omega (u_i)^* (\hat{v}_g^P)_j C_{ijkl} s_{kl}, \quad (2d)$$

$$\alpha = \Omega^2 \mathcal{I}_A^{-1} s_{ij} \eta_{ijkl} (s_{kl})^*, \quad (2e)$$

respectively, where ε_{ij} is the relative permittivity tensor, u_k is the acoustic displacement from equilibrium, $E^{P,S}$ and $H^{P,S}$ are the electric and magnetic field vectors for the pump and Stokes fields, respectively. Additionally, \hat{v}_g^P is the normalised group velocity for the pump field, ε_{ijk} is the Levi-Civita tensor, C_{ijkl} is the stiffness tensor, and η_{ijkl} is the phonon viscosity tensor. Finally, ω and Ω are the angular frequencies of the pump field and the acoustic wave, respectively, and $s_{kl} = (\partial_k u_l + \partial_l u_k)/2$ is the linear strain tensor. Here we define P_{ijkl} via [24]

$$\Delta\varepsilon_{ij} = -\varepsilon_{im}\varepsilon_{jn}P_{(mn)kl}\partial_l u_k, \quad (3a)$$

where the full photoelastic tensor decomposes as

$$P_{(ij)kl} = p_{(ij)(kl)} + p_{(ij)[kl]}, \quad (3b)$$

for non-piezoelectric dielectric materials, with $p_{(ij)(kl)}$ and $p_{(ij)[kl]}$ denoting the symmetric and antisymmetric (roto-optic) photoelastic tensors, respectively. Following [24], we represent index pair interchange symmetry with

parentheses and interchange antisymmetry with square brackets. Note that (3b) represents a key departure from conventional treatments of SBS, as $p_{(ij)[kl]} \equiv 0$ in optically isotropic materials [25].

To evaluate (1), it is necessary to determine a large number of modal fields belonging to several different families. For determining the optical fields and quantities in (2), such as wave polarisations and the refractive index, we consider Maxwell's equations with the plane wave ansatz $E_j = \tilde{E}_j \exp(ik_i x_i - i\omega t)$ where \tilde{E}_j denotes the polarisation of the wave, and k_j is the wave vector. This ansatz admits the system [26]

$$\left(\hat{k}_i \hat{k}_j - \left(1 - \frac{\varepsilon_j}{n^2}\right) \delta_{ij}\right) \tilde{E}_j = A_{ij}^M \tilde{E}_j = 0, \quad (4)$$

where $k_i = k \hat{k}_i$, $k = n\omega/c_0$ is the wave number, n is the refractive index, and c_0 denotes the speed of light in vacuum. Subsequently, for a given wave vector k_j , the supported refractive indices are obtained by solving $\det(A^M) = 0$ and the associated eigen-polarisations \tilde{E}_j are given by the eigenvectors of A^M . The corresponding group velocity of the wave ($[v_g]_i = \partial_{k_i} \omega$) is obtained by implicit differentiation of (4).

In order to determine the properties of the available Stokes waves for a given pump wave vector k_j^P , namely the wave vectors k_j^S and wave polarisations \tilde{E}_j^S , we impose that the direction of the group velocity vector for the Stokes wave is opposite in sign to that of the pump wave ($[\hat{v}_g^S]_j = -[\hat{v}_g^P]_j$), which is consistent with backwards SBS coupling. From this group velocity condition, the properties of the Stokes wave are obtained following the procedure above for the pump wave.

To determine acoustic fields and quantities, we consider the acoustic wave equation [8] assuming the plane wave ansatz $u_j = \tilde{u}_j \exp(iq_i x_i - i\Omega t)$, where \tilde{u}_j is the polarisation, and the acoustic wave vector q_j is defined by $q_j = k_j^P - k_j^S = q\hat{q}_j$ [4, 5]. Subsequently, we obtain the eigenvalue problem

$$A_{ij}^A v_j = \frac{\rho\Omega^2}{q^2} v_i, \quad (5)$$

which returns $\rho\Omega^2/q^2$ as eigenvalues and \tilde{u}_j as eigenvectors, where ρ denotes the mass density and $v_j = \partial_t u_j$ the phase velocity of the wave. The Christoffel tensor A_{ij}^A is widely tabulated for a broad selection of Bravais lattice classes [8, 27, 28].

We now proceed to a numerical study examining the SBS performance of Si-As₂S₃ layered media with a unit cell length of 50 nm and at a vacuum wavelength $\lambda_0 = 1550$ nm. Even though the layered media consists of an acoustically isotropic and cubic medium, the composite medium is optically uniaxial. In Eqs. (1)-(3b) above, we use the closed-form expressions for ε_{ij} , C_{ijkl} , η_{ijkl} , ρ , and $P_{(ij)kl}$ derived in Smith *et al.* [16] for laminate materials possessing tetragonal ($4/mmm$) symmetry (i.e., when the constituent layers possess isotropic or cubic symmetry). These descriptions are valid provided the wavelengths of all optical and acoustic waves are much longer

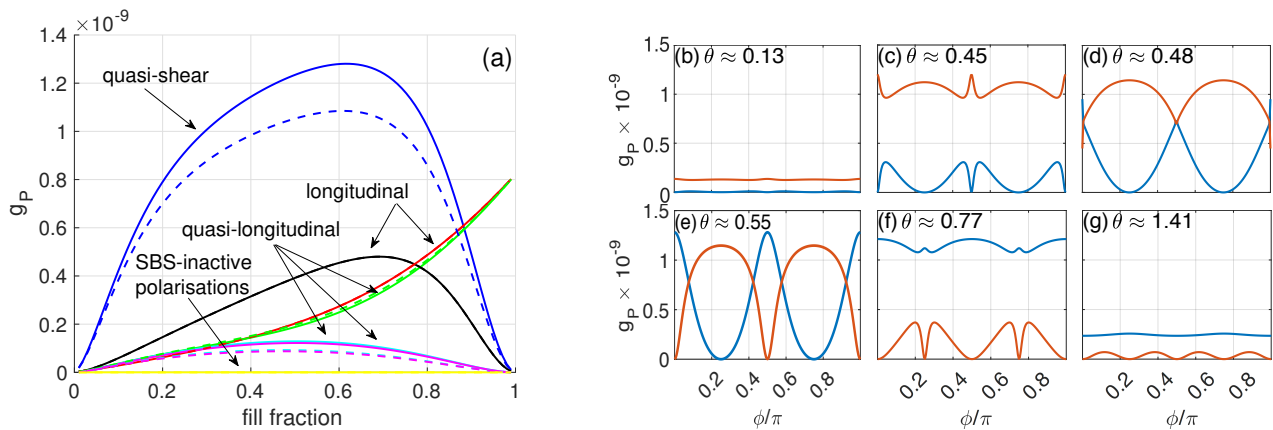


FIG. 2. SBS gain coefficient for As_2S_3 -Si layered medium as (a) function of filling fraction f for fixed pump wave vector $k^{\text{P}} \approx (0.52, 0, 0.85)$. Dashed curves are gain values when roto-optic contributions are neglected (i.e., $p_{ij[kl]} = 0$). Each curve represents different combinations (branches) of pump, Stokes, and acoustic waves (i.e., blue = quasi-shear, red = longitudinal acoustic wave polarisations); (b-g) function of $k^{\text{P}} = (\sin \theta \cos \phi, \sin \theta \sin \phi, \cos \theta)$ at $f \approx 0.61$. Two competing mixed acoustic mode branches are shown (remaining branches omitted for clarity). In all figures we consider a period of 50 nm.

than the periodic length scale of the laminate; in this regime the behaviour of the composite material is accurately described by an effective uniform material. Material constants for the constituent layers are given in Smith *et al.* [13].

For the tetragonal laminates we consider, two pump waves are generally supported for wave vectors oriented away from directions of high symmetry (one for the extraordinary and another for the ordinary surface). Thus, for a specified \hat{k}^{P} in a bulk uniaxial crystal, up to four pair combinations of pump and Stokes waves may contribute to an SBS process. For each combination of pump and Stokes wave field, there are up to three acoustic wave polarisations supported at long wavelengths, giving a total of twelve possible combinations of pump, Stokes, and acoustic waves to participate in an SBS process in a tetragonal ($4/mmm$) material for a given \hat{k}^{P} . In a composite material, the symmetric photoelastic tensor defined in (3b) may be decomposed further as

$$p_{(ij)(kl)} = p_{(ij)(kl)}^{\text{pe}} + p_{(ij)(kl)}^{\text{art}}, \quad (6)$$

representing some weighted average of constituent photoelastic terms and artificial photoelasticity coefficients, respectively [16].

In Fig. 2(a) we present the gain coefficient as a function of filling fraction for all twelve possible combinations of pump, Stokes, and acoustic wave polarisations (henceforth we refer to each of these twelve combinations as *branches*) corresponding to $k^{\text{P}} \approx (0.52, 0, 0.85)$. This particular wave vector corresponds to the maximum possible gain value of $\max(g_{\text{P}}) = 1.28 \times 10^{-9} \text{ W}^{-1} \text{ m}$ for this material pair, which occurs at $f \approx 0.61$ (note that two other k^{P} orientations return the same $\max(g_{\text{P}})$, see below). Superimposed on this figure are the twelve branches for this structure when roto-optic contributions are neglected, returning a maximum gain value of

$g_{\text{P}} = 1.08 \times 10^{-9} \text{ W}^{-1} \text{ m}$ at $f \approx 0.61$, and ultimately revealing a roto-optic enhancement of 19% to the $\max(g_{\text{P}})$. These dashed curves also allow us to identify the shear contribution to each mode as a function of filling fraction, revealing that the medium-gain branches (depicted by the black, red, and green curves in Fig. 2(a)) are almost purely longitudinal acoustic modes, for example. At filling fractions of approximately 88% and higher, the greatest gain value is achieved for a longitudinally polarised acoustic mode (red curve), which is the only acoustic polarisation that is SBS-active in isotropic materials. Recall that pure $\text{Si}100\bar{j}$, corresponding to $f = 0\%$, possesses an intrinsically low SBS performance with $g_{\text{P}} = 2.4 \times 10^{-12}$ [13]. At $f = 100\%$ we obtain $g_{\text{P}} = 8.02 \times 10^{-10} \text{ W}^{-1} \text{ m}$ for pure As_2S_3 , which is marginally higher than experimental results ($g_{\text{P}} = 7.4 \times 10^{-10} \text{ W}^{-1} \text{ m}$ in As_2S_3) [17]. Note also that half of the available mode branches are not SBS-active for any filling fraction. If we decompose the total electrostrictive coefficient in (1) as $\gamma = \gamma^{\text{pe}} + \gamma^{\text{art}} + \gamma^{\text{ro}}$, where γ^{pe} refers to intrinsic photoelastic contributions alone, γ^{art} artificial contributions alone, and γ^{ro} the gain due to roto-optic contributions alone, we find that these quantities amount to 74%, 18%, and 8% of the overlap for the maximum gain value observed in Fig. 2(a), respectively. The modest contributions γ^{art} and γ^{ro} are responsible for significant increases in the gain following (1), and highlight the importance of accurately capturing all optomechanical processes for SBS calculations in composites. To summarise, we find a maximum gain of $g_{\text{P}} = 1.28 \times 10^{-9} \text{ W}^{-1} \text{ m}$ at $k^{\text{P}} \approx (0.52, 0, 0.85)$ and $f \approx 0.61$, where $\Omega/(2\pi) = 8.4 \text{ GHz}$, $\alpha = 16665 \text{ m}^{-1}$, $v_{\text{g}}^{\text{A}} = 2353 \text{ m/s}$ and $k^{\text{S}} = -k^{\text{P}}$ (materials tensors are also summarised in Table I).

In Figs. 2(b-g), we consider the gain coefficient at fixed filling fraction $f \approx 0.61$ as we examine the parameter space for the pump wave vector, i.e. for $k^{\text{P}} = (\sin \theta \cos \phi, \sin \theta \sin \phi, \cos \theta)$, where ϕ is measured relative

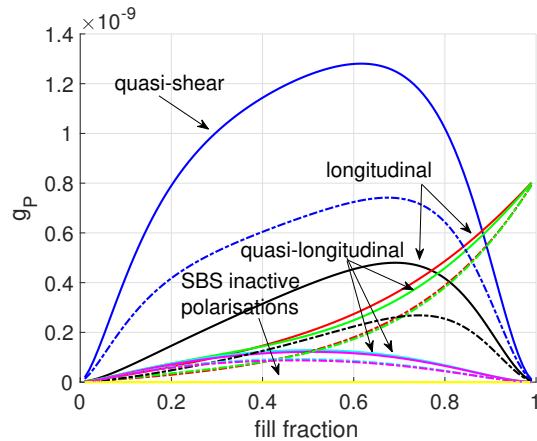


FIG. 3. SBS gain coefficient as function of f for As_2S_3 -Si layered medium shown in Fig. 2(a) where results for neglected roto-optic and artificial photoelastic contributions (i.e., both $p_{ij[kl]} = 0$ and $p_{ij(kl)}^{\text{art}} = 0$) are overlaid (dot-dash curves).

to the $\langle 100 \rangle$ axis of Si and the layers are stacked along $\langle 001 \rangle$. Specifically, we present the gain along ϕ (equatorial plane) as we sweep meridional angles θ . In this instance, only the two largest and competing branches are shown for clarity. These figures clearly demonstrate the importance of correctly orienting the pump wave vector, as particular orientation angles correspond to gain suppression (i.e., at $\theta \approx 0.45$ and $\phi = \pi/2$), and that the maximum gain value occurs not only at a single pump wave vector. That is, the maximum SBS gain is achieved at three pump wavevectors corresponding to $\phi = 0, \pi/2, \pi$ with $\theta \approx 0.55$. For $\theta \approx 0.55$ the maximum gain branch (blue curve) shows that the incident wave vector must be appropriately oriented to achieve maximal results, however, the presence of the second acoustic branch (red curve) ensures that the gain coefficient does not take values beneath $g_P \approx 7.8 \times 10^{-10} \text{ W}^{-1} \text{ m}$. Interestingly, all figures demonstrate the intense competition between acoustic mode branches for the maximum gain position, in addition to revealing intrinsic symmetries for the gain parameter in layered media as a function of the

k^P direction.

In Fig. 3 we examine the gain coefficient for the layered medium ($f = 0.61$) along $k^P \approx (0.52, 0, 0.85)$, when both roto-optic and artificial photoelastic contributions are neglected. Also superimposed are the total gain coefficient curves from Fig. 2(a) for reference. Here, we find that the estimated gain for layered media in the absence of these two contributions is significantly reduced (in particular, the maximum gain occurs at $f \approx 0.67$ with $g_P = 7.4 \times 10^{-10} \text{ W}^{-1} \text{ m}$). At $f \approx 0.61$ we find $g_P = 7.3 \times 10^{-10} \text{ W}^{-1} \text{ m}$ and subsequently establish that artificial and roto-optic effects increase the maximum SBS gain coefficient observed in Fig. 2(a) by approximately 75%.

In summary, we have presented a theoretical framework for investigating SBS in anisotropic materials, and using this framework we propose a nanoscale layered material with an SBS coefficient that outperforms leading materials platforms. The structure we propose represents an enhancement in the SBS performance of silicon by more than two orders of magnitude, and is achieved by incorporating contributions from the symmetric photoelastic tensor (containing artificial photoelastic contributions only present in composite media), as well as contributions from the antisymmetric photoelastic tensor (roto-optic tensor), where the latter effect arises in all optically anisotropic media. We have also shown that artificial photoelastic and roto-optic contributions are non-negligible in optically anisotropic materials, contributing significantly to the total gain coefficient for our Si- As_2S_3 structure. For this material pair, the gain coefficient of the layered medium is larger than that of the embedded array medium [14], due to stronger artificial contributions and the emergence of roto-optic contributions. The framework presented here provides extensive scope for the ongoing development of new materials for future photonics and optomechanics research.

Funding. Australian Research Council (ARC) (CE110001018, DP160101691). C. Wolff acknowledge funding from MULTIPLY fellowships under the Marie Skłodowska-Curie COFUND Action (grant agreement No. 713694).

-
- [1] R. van Laer, B. Kuyken, D. van Thourhout, and R. Baets, *Nat. Photon.* **9**, 199 (2015).
 - [2] O. Florez, P. F. Jarschel, Y. A. Espinel, C. Cordeiro, T. M. Alegre, G. S. Wiederhecker, and P. Dainese, *Nat. Comm.* **7**, 11759 (2016).
 - [3] N. T. Otterstrom, R. O. Behunin, E. A. Kittlaus, Z. Wang, and P. T. Rakich, *Science* **360**, 1113 (2018).
 - [4] R. W. Boyd, *Nonlinear optics* (Elsevier, New York, 2003).
 - [5] P. E. Powers, *Fundamentals of nonlinear optics* (CRC Press, Boca Raton, 2011).
 - [6] B. J. Eggleton, C. G. Poulton, and R. Pant, *Adv. Opt. Photon.* **5**, 536 (2013).
 - [7] D. F. Nelson and P. D. Lazay, *Phys. Rev. Lett.* **25**, 1187 (1970).
 - [8] B. A. Auld, *Acoustic fields and waves in solids* (John Wiley & Sons, Toronto, 1973).
 - [9] D. F. Nelson and P. D. Lazay, *Phys. Rev. B* **16**, 4659 (1977).
 - [10] C. Wolff, M. J. Steel, and C. G. Poulton, *Opt. Exp.* **22**, 32489 (2014).
 - [11] M. J. A. Smith, B. T. Kuhlmeier, C. M. de Sterke, C. Wolff, M. Lapine, and C. G. Poulton, *Phys. Rev. B* **91**, 214102 (2015).
 - [12] W. Sun, S. Wang, J. Ng, L. Zhou, and C. T. Chan, *Phys. Rev. B* **91**, 235439 (2015).

- [13] M. J. A. Smith, B. T. Kuhlmeier, C. M. de Sterke, C. Wolff, M. Lapine, and C. G. Poulton, *Opt. Lett.* **41**, 2338 (2016).
- [14] M. J. A. Smith, B. T. Kuhlmeier, C. M. de Sterke, C. Wolff, M. Lapine, and C. G. Poulton, *J. Opt. Soc. Am. B* **33**, 2162 (2016).
- [15] X.-X. Su, X.-S. Li, Y.-S. Wang, and H. P. Lee, *J. Opt. Sci. Am. B* **34**, 2599 (2017).
- [16] M. J. A. Smith, C. M. de Sterke, C. Wolff, M. Lapine, and C. G. Poulton, *Phys. Rev. B* **96**, 064114 (2017).
- [17] R. Pant, C. G. Poulton, D.-Y. Choi, H. Mcfarlane, S. Hile, E. Li, L. Thevenaz, B. Luther-Davies, S. J. Madden, and B. J. Eggleton, *Opt. Exp.* **19**, 8285 (2011).
- [18] R. A. Toupin, *J. Ration. Mech. Anal.* **5**, 849 (1956).
- [19] D. F. Nelson and P. D. Lazay, *Phys. Rev. Lett.* **25**, 1638 (1970).
- [20] D. F. Nelson, *Electric, optic, and acoustic interactions in dielectrics* (John Wiley & Sons, New York, 1979).
- [21] R. Vacher and E. Courtens, in *International Tables for Crystallography*, Vol. D, edited by A. Authier (International Union of Crystallography, Chester, 2006) Chap. 2.4, pp. 329–335.
- [22] C. Wolff, M. J. Steel, B. J. Eggleton, and C. G. Poulton, *Phys. Rev. A* **92**, 013836 (2015).
- [23] C. Wolff, R. Soref, C. G. Poulton, and B. J. Eggleton, *Opt. Exp.* **22**, 30735 (2014).
- [24] D. F. Nelson and M. Lax, *Phys. Rev. Lett.* **24**, 379 (1970).
- [25] D. F. Nelson, P. D. Lazay, and M. Lax, *Phys. Rev. B* **6**, 3109 (1972).
- [26] M. Born and E. Wolf, *Principles of optics: electromagnetic theory of propagation, interference and diffraction of light* (Pergamon Press, New York, 1964).
- [27] J. F. Nye, *Physical properties of crystals: their representation by tensors and matrices* (Oxford university press, Suffolk, 1985).
- [28] R. E. Newnham, *Properties of Materials: Anisotropy, Symmetry, Structure* (Oxford University Press, New York, 2004).

TABLE I. **Bulk values for relative permittivity ε_j , stiffness C_{ij} (units [GPa]), phonon viscosity η_{ij} (units [mPa · s]), density ρ (units [kg · m⁻³]), symmetric photoelastic $p_{i(j)}$, and roto-optic $p_{i[j]}$ tensors of layered medium ($f = 0.61$). Subscripts are in Voigt form and $p_{i(j)} = p_{i(j)}^{\text{pe}} + p_{i(j)}^{\text{art}}$.**

Physical quantity	ε_1	ε_3	C_{11}	C_{33}	C_{13}	C_{12}	C_{44}	C_{66}	η_{11}	η_{33}	η_{13}	η_{12}	η_{44}	η_{66}	ρ
Effective parameter	8.11	7.08	68.2	28.4	9.9	21.1	9.9	34.6	2.63	2.46	2.05	2.13	0.25	0.35	2864
Physical quantity	$p_{1(1)}$	$p_{3(3)}$	$p_{1(3)}$	$p_{1(2)}$	$p_{3(1)}$	$p_{4(4)}$	$p_{6(6)}$	$p_{1(1)}^{\text{art}}$	$p_{3(3)}^{\text{art}}$	$p_{1(3)}^{\text{art}}$	$p_{1(2)}^{\text{art}}$	$p_{3(1)}^{\text{art}}$	$p_{4[4]}$		
Effective parameter	0.015	0.258	0.143	0.107	0.209	-0.0004	-0.0422	0.012	0.03	0.031	0.012	0.012	0.009		